



HAL
open science

Vibration Analysis for Damage Detection in Ultra filtration Fibers

Julien Roussel, Philippe Ravier, Cécile Capdessus, Meryem Jabloun

► **To cite this version:**

Julien Roussel, Philippe Ravier, Cécile Capdessus, Meryem Jabloun. Vibration Analysis for Damage Detection in Ultra filtration Fibers. *Surveillance* 6, Oct 2011, Compiègne, France. hal-00652191

HAL Id: hal-00652191

<https://hal.science/hal-00652191>

Submitted on 15 Dec 2011

HAL is a multi-disciplinary open access archive for the deposit and dissemination of scientific research documents, whether they are published or not. The documents may come from teaching and research institutions in France or abroad, or from public or private research centers.

L'archive ouverte pluridisciplinaire **HAL**, est destinée au dépôt et à la diffusion de documents scientifiques de niveau recherche, publiés ou non, émanant des établissements d'enseignement et de recherche français ou étrangers, des laboratoires publics ou privés.

Vibration Analysis for Damage Detection in Ultra filtration Fibers

J. Roussel*, P. Ravier*, C. Capdessus**, M. Jabloun*

* PRISME laboratory, Polytech'Orléans, 12 rue de Blois - BP 6744 - 45067 Orléans cedex 02, France

** PRISME laboratory, 21 Rue Loigny la Bataille, 28000 Chartres, France

julien.rousseau@gmail.com

{Philippe.Ravier ; Cecile.Capdessus ; Meryem.Jabloun}@univ-orleans.fr

Abstract

This paper concerns the monitoring of water ultra-filtration devices by vibration analysis. Damaged devices are characterized by the presence of air bubbles that can be heard by a trained service engineer. The present study investigates the feasibility of an automated detector that could complete the engineer's expertise. A description of the filtration devices is given and the main features of the transients to be detected and the ambient noise are brought to light. Based on these features, six detectors are proposed. They are tested and compared through Monte Carlo simulations over data built from real life signals.

Keywords

Water filtration, bubbles, transient signals, detection, vibration analysis

1. Introduction

Ultrafiltration using hollow fibers is a commonly used method for drinking water production because it allows removing micro particles up to ten nanometers and pathogens without using chemicals. Fibers are organized like spaghettis inside ultrafiltration modules (tubes). High pressure water is injected through the fibers. Part of it runs through the fibers membranes and reaches the inside of the module as pure as source water. However, due to the high water pressure, fibers may be damaged, causing the dirty water to reach the module and be mixed with the pure water.

Some integrity tests have been investigated that induce the dismantling of modules [GUO10], which requires time and money. Moreover water analysis methods do not allow determine which module is damaged within the set of modules [GUO10].

The diagnosis technique used in practice consists in injecting air into the fibers within a water filled module. The air is normally stopped by the fiber membrane but in the presence of a damaged fiber, the air passes through this damaged fiber creating some bubbles inside the module. This bubble emission exhibits a recognizable acoustic signature, a transient signal, which can be used for detection purpose. Currently skilled technicians listen to these bubble sounds in order to report on the module state but the subjectivity of this test may induce both detection errors and improper estimation of damages.

Time and money could be saved with an on-line based fault diagnosis system that would be able to automatically detect bubbles and therefore to identify damaged modules. Such a system would not need to stop water production but would only require integration of equipments into or on the modules. However, for this system, a correct identification of damaged modules is essential and depends on the quality of the transient detectors.

The purpose of this study is hence to investigate for an efficient automated bubble detection technique.

To fulfill this goal, *in-situ* measurements are carried out for precise transients and noise characterization. Transient types can therefore be identified. Appropriate detectors are then proposed and their performance is evaluated.

The experimental setup is described in section 2. In section 3, both noise and transients are characterized. In section 4, performance detection curves are presented for each transient type with the proposed detection methods and detection curves are shown on a real life signal.

2. Experimental Setup

2.1. Sensor selection

Microphone seems to be a natural way to replace human ear. However, the noisy environment of the modules makes accurate measurements difficult. In addition, the pressure wave crosses multiple medium interfaces: water to module wall, module wall to air and air to microphone membrane. Accelerometers actually appear to be better fitted to the case. Firstly, they reduce the number of interfaces by two: water to wall and wall to accelerometer. Secondly, they reproduce what happens when the technician sticks his ear to the module, *i.e.* the vibration is directly transmitted to the inner ear by the *cranium* bones. For those reasons and based on preliminary experiments, the system has been chosen to be based on vibration analysis rather than sound analysis.

The selected sensor is a high sensitivity integrated circuit piezoelectric accelerometer (ICP) Kistler 8786A5 with a range of ± 5 g, a sensitivity of 1000 mV/g and a bandwidth of 6 kHz. The sensor is fixed on the module with a special wax.

2.2. Acquisition Chain

The data acquisition setup is composed of the following parts (Figure 1):

- A high sensitivity accelerometer.
- A signal conditioner MEIRI ME2680 with an ICP sensor amplifier card ME26C-ICP. The amplifier has an adjustable gain between 1 and 20, an adjustable output range up to 10V and a bandwidth of 30 kHz.
- A National Instrument data acquisition card NI PCI-4472 composed of eight 24-bit analog to digital delta-sigma converters at a maximum of 102400 samples per second, with an alias-free bandwidth of 45 kHz.
- A computer with Labview environment.

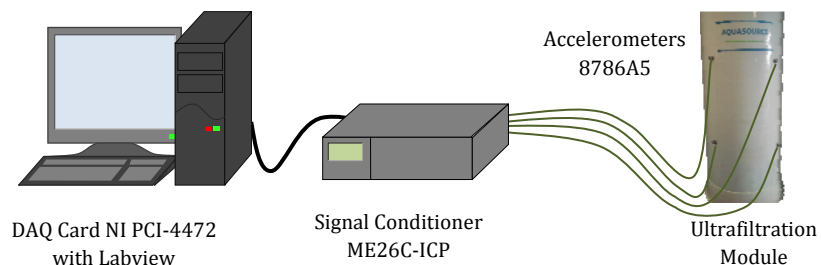


Figure 1: Data Acquisition Chain.

2.3. Measurements

Preliminary measurements on damaged modules show a maximum useful frequency at 5 kHz. So, in order to maintain a good signal quality, a sampling frequency of 50 kHz has been chosen. The voltage gain of instrumentation amplifier has been adjusted to maximize the output voltage at ± 10 V, with a value of 13.33. So we have a full measurement range of ± 750 mg. The 24 bits analog to digital converter provides a quantum of 0.089 μ g.

A database has been established with damaged and undamaged modules measurements during the integrity test process. Each measurement is associated to an information file with the module serial number and its location inside the plant. On each damaged module, two measurements have been made, one before repairing and one afterwards.

The identification of damaged modules is primarily based on the presence of bubbles that have to be detected as transient signals buried in ambient noise. In order to develop detection procedures in the classical binary hypothesis testing way, the noise and added transients have to be characterized.

3. Noise and Transient Signals Characterization

3.1. Noise

3.1.1. Histogram

First, in order to characterize the noise inside a module, some records have been made from undamaged modules. A statistical study performed over temporal signals shows a Gaussian distribution of this background noise as displayed in Figure 2. The standard deviation may vary according to the production or module position but is generally around 10 to 50 mg.

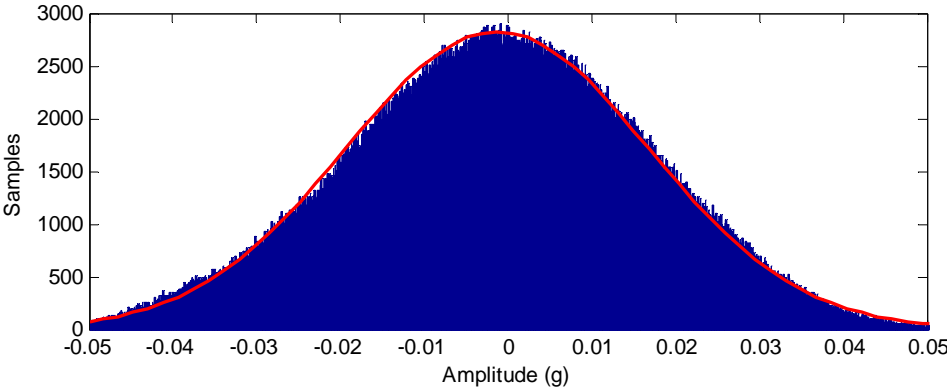


Figure 2: Histogram of the temporal vibration recorded on an undamaged device (20 s duration). The blue plot represents the data histogram while the red one represents Gaussian fit of the histogram,

3.1.2. Background noise

The power spectral density of the records, using Welch's averaged periodogram with a 10 ms rectangular window, exhibits two pink noises at -60 dB/dec up to 800 Hz and -10 dB/dec at higher frequencies (Figure 3). Figure 4 displays the time-frequency representation of this noise calculated with a short-time Fourier transform using a Hanning window of 1 s.

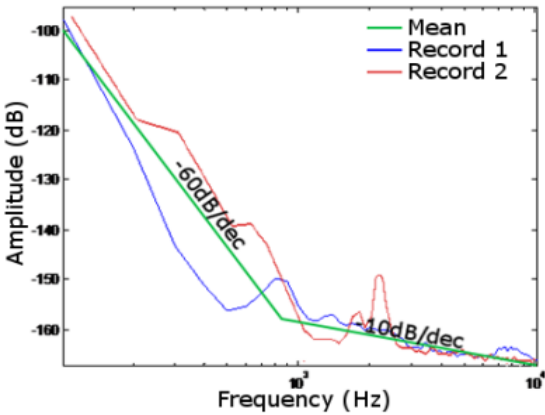


Figure 3: Noise Power Spectral Density, estimated on 20 s duration records. The sampling frequency is 50 kHz.

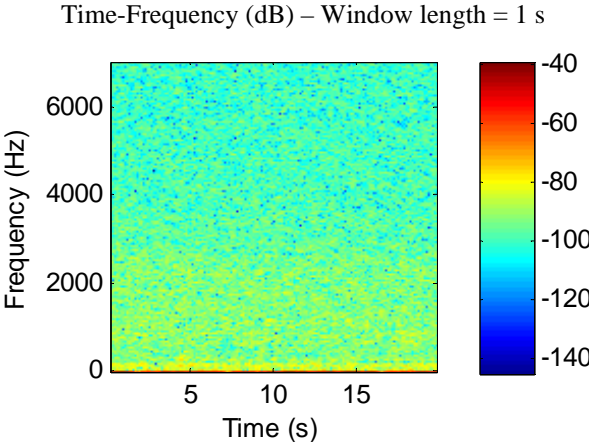


Figure 4: Noise Spectrogram.

3.1.3. Engine noise

We can also note the presence of constant frequencies along some signals. Figure 5 and Figure 6 show the spectrograms of an undamaged module with some components at 300, 800, 900, 1400, 1700, 2800 and 3400 Hz. This unfavorable case is not permanent since all these frequencies are induced by the pumps used during the filtration process.

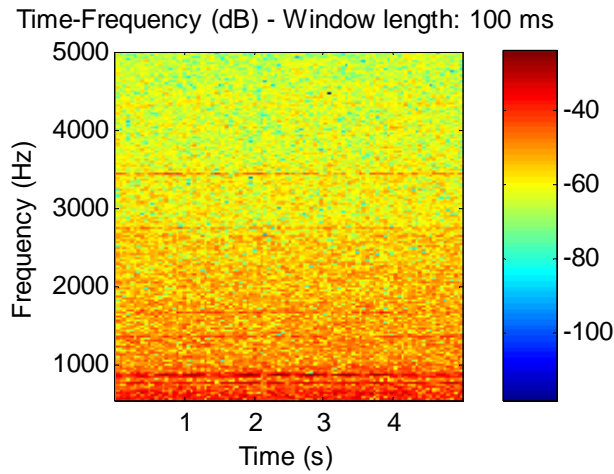


Figure 5: Noise Spectrogram (550 to 5000 Hz). The observed pure tones are caused by pumps.

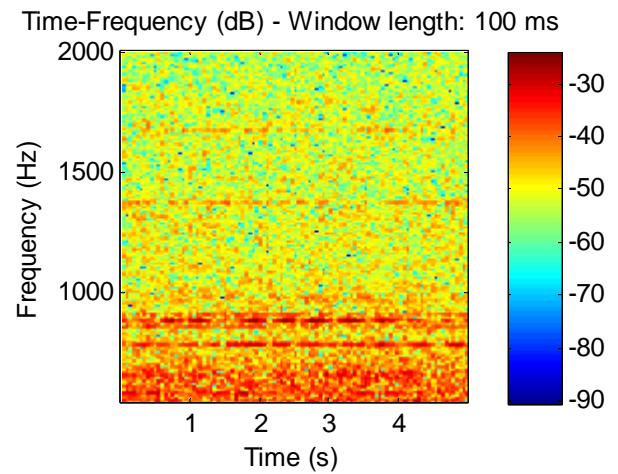


Figure 6: Noise Spectrogram (550 to 2000 Hz). Pumps are the major contributions to the observed pure tones.

3.2. Transients

Secondly, we have identified phenomena inside damaged modules: different kinds of transients were observed. We have classified them into five categories, depending on their time-frequency features and the corresponding sound that can be heard when sending the vibration signal to a loudspeaker. In what follows, these five categories will be denoted types {A, B, C, D, E} and labeled {"glou-glou", "slup", "tic-tic", "tac-tac", "tap-tap"} sounds, respectively. Figure 7 is a spectrogram example of a damaged module. Repetitive events are mostly observed. Depending on the types, the events can either be narrow band mono-component transients (Figure 8-a) or multi-component transients (Figure 8-b). Mono-component transients are composed of one central frequency which may vary (Figure 8-a, center frequency of $1 \text{ kHz} \pm 200 \text{ Hz}$). Multi-component transients are constituted of several local central frequencies that are synchronized or not (Figure 8-b, center frequency between 200 Hz and 2 kHz). Note that the sounds produced by these multi component transients are characteristic of bubble pops.

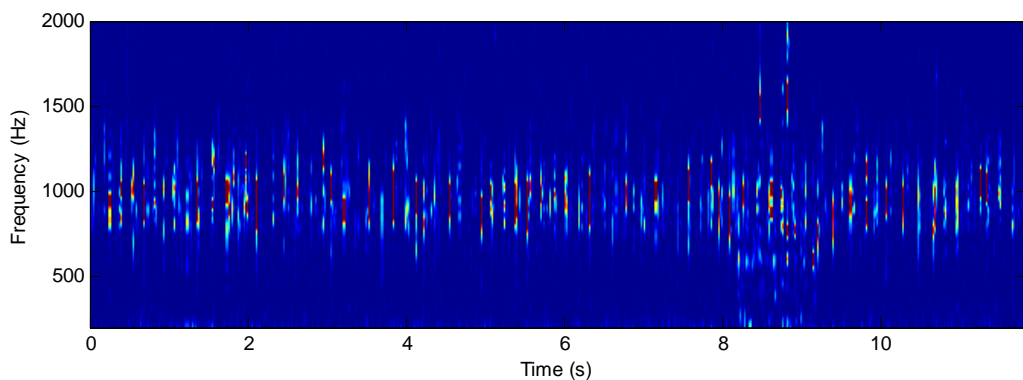


Figure 7: Spectrogram of one damaged module.

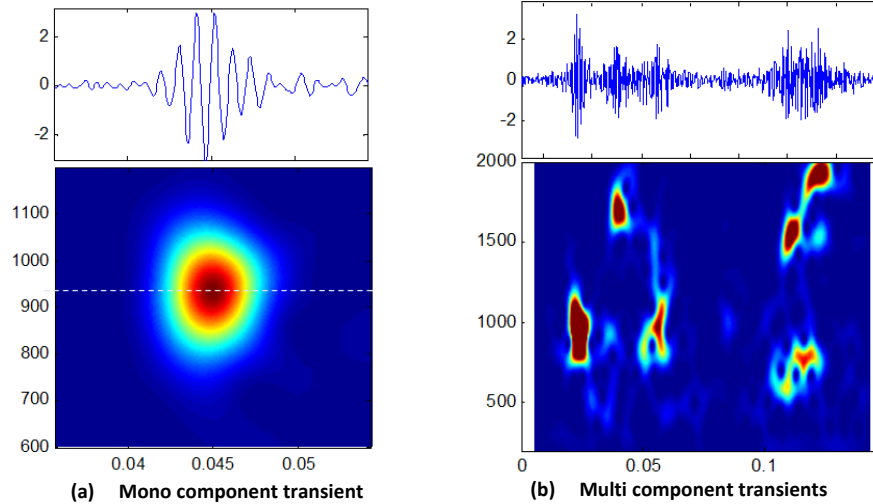


Figure 8: Temporal representation and spectrogram of two transient types.

In Figures 9-a to 9-e the five different types of transients are exposed through their temporal representation, their spectrogram and their temporal histogram. In many cases, the distribution is far from the Gaussian one (cases when the normalized kurtosis value K_4 is far from the 0 value [NIK93]).

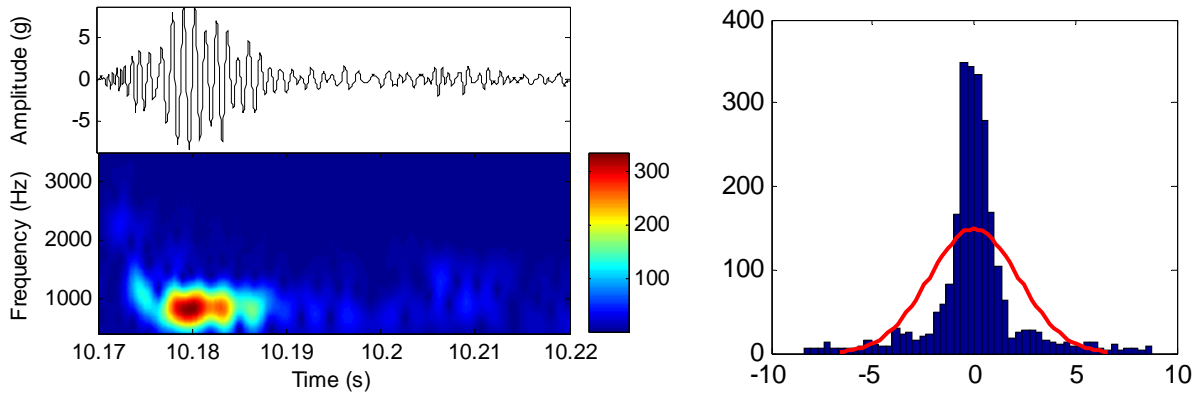


Figure 9 - a: Spectrogram and temporal histogram of the type A transient (*glou-glou*), $K_4 = 4.1$

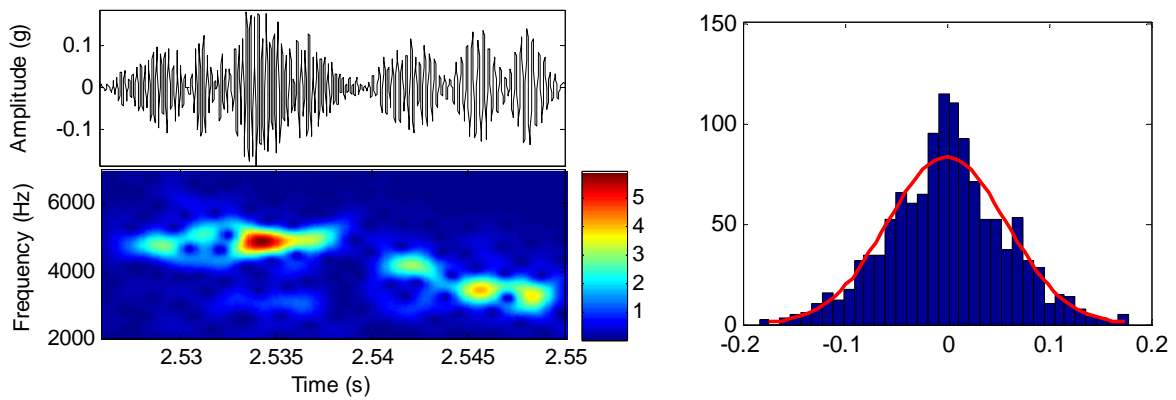


Figure 9 - b: Spectrogram and temporal histogram of the type B transient (*slup*), $K_4 = 0.2$

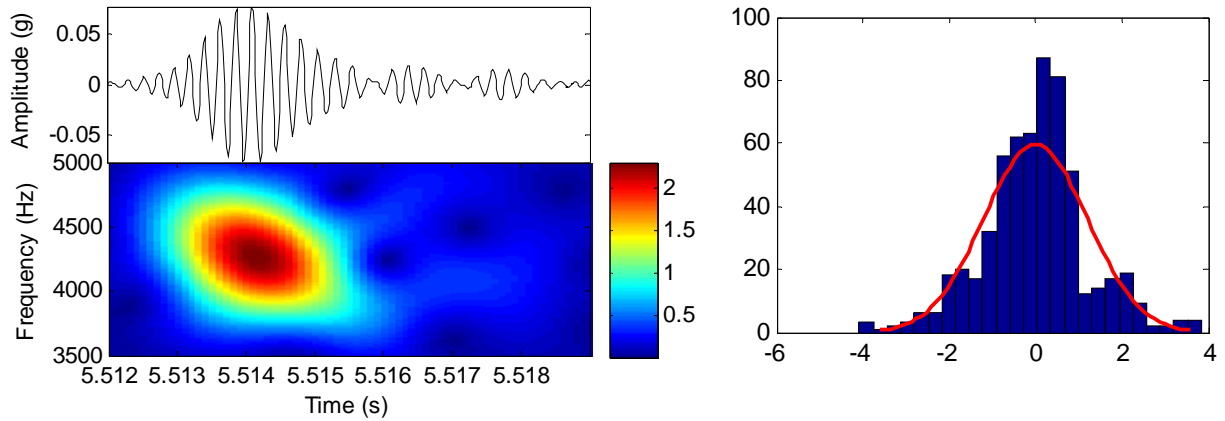


Figure 9 - c: Spectrogram and temporal histogram of the type C transient (*tic-tic*), $K_4 = 1.1$

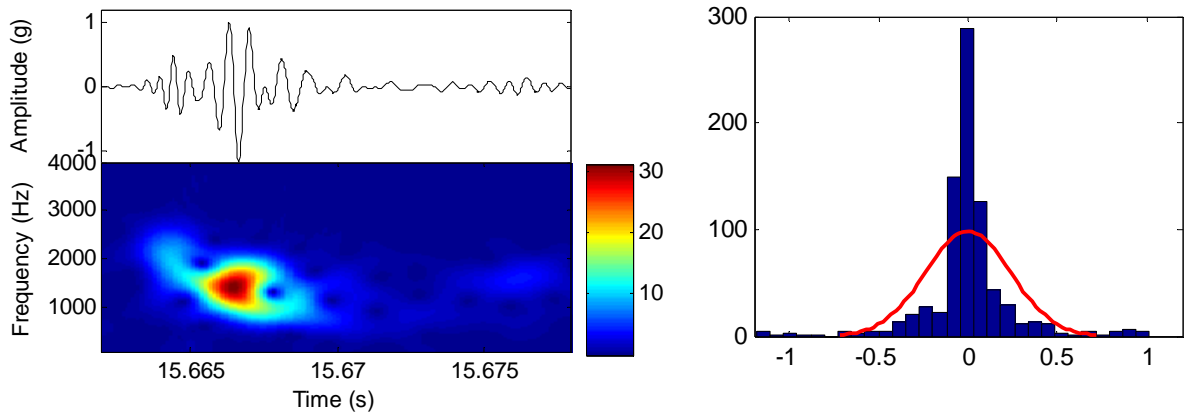


Figure 9 - d: Spectrogram and temporal histogram of the type D transient (*tac-tac*), $K_4 = 7.3$

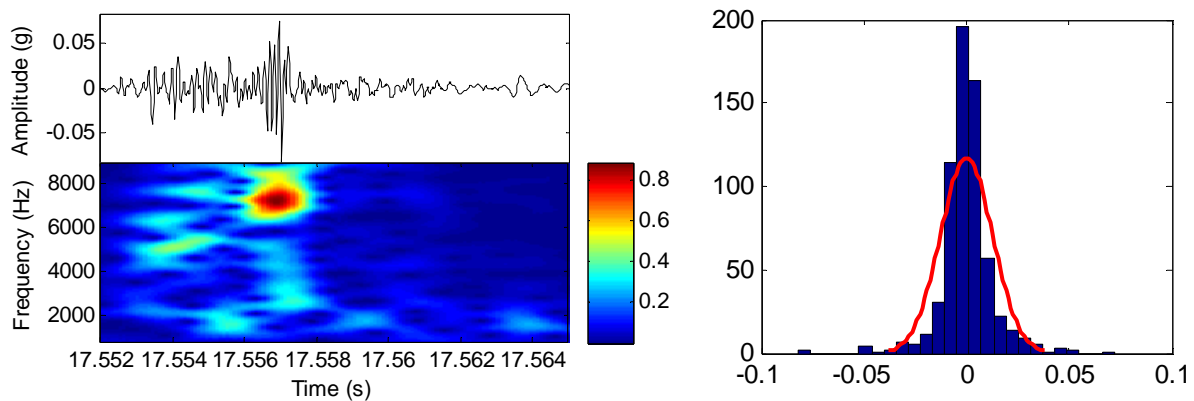


Figure 9 - e: Spectrogram and temporal histogram of the type E transient (*tap-tap*), $K_4 = 8.8$

4. Proposed detection techniques and test method

Based on noise and signal features, several detectors can be proposed. First, as can be seen on the transients spectrograms as well as on their temporal representation, the bubbles produce local bursts of energy. The simplest detector is thus based on the energy calculation. Second, it was shown both by time and frequency analysis and by ear study coupled with different band pass-filters, that bubbles are located above 800 Hz, while

the noise exhibits very strong energy at low frequencies. Therefore, a high-pass filter can be applied to the signal prior to the energy detector. Third, the magnitude distribution of many transients deviates from Gaussianity as it is shown on the histogram plots of section 3.2, whereas the noise exhibits the Gaussian property. Thus higher order statistics, for example the fourth-order cumulant, can be used to measure deviations from Gaussianity. Fourth, the signals of interest are naturally non-stationary, so that time-frequency or time/scale representations are dedicated tools to properly analyze these data. We tested adaptive segmentation in the time domain using Malvar wavelet decomposition [Rav98] and adaptive segmentation in the frequency domain using wavelet packet decomposition [Rav01].

The selected detectors as well as the test method will be more precisely described in the following parts, while the experimental results will be given in the last part of this section.

4.1. Energy detector

Let us denote by $x(n)$ the n^{th} sample of the observation, and N the total number of samples. The energy $E(n)$ is adaptively estimated using the following expression:

$$E(n) = E(n-1) + \mu \cdot (x^2(n) - E(n-1)), \quad \forall n \in [2; N] \quad (1)$$

where the initial energy is set as $E(1) = x^2(1)$. The adaptive step can be any $\mu \in [0; 1]$, and it is to be chosen by taking into account the duration of the transients. In what follows, this step is fixed to $\mu = 0.1$ for all experiments.

4.2. Energy detector with prior filtering

The preliminary study showed that transients are located above 800 Hz, while the noise energy dramatically decreases with frequency. Therefore it is interesting to apply a high-pass filter to the data prior to the detection. The second detector is thus the combination of a butterworth high-pass filter at frequency 500 Hz followed by the energy detector.

4.3. Fourth-order moment with prior filtering

This detector aims at detecting deviations from Gaussian property. A second-order estimator (energy estimator) is not sufficient to detect nonGaussian events. For that purpose, higher-order statistics are often used. In particular, the normalized kurtosis value which is a normalized value of the fourth-order cumulant, is known to be zero when the process is Gaussian. Let us recall the definition of the normalized kurtosis value K_4 . For any zero-mean random variable X describing the process, K_4 writes:

$$K_4 = \frac{\mathcal{E}\{X^4\}}{\mathcal{E}\{X^2\}^2} - 3 \quad (2)$$

with \mathcal{E} representing the mathematical expectation. The normalization factor is the energy whose online estimation may thoroughly impact the kurtosis estimated value. A simple way to estimate K_4 is to normalize the variable with respect to the total energy of the observation before estimation. So, for this detector, the K_4 estimation is reduced to the simple online M_4 fourth-order moment:

$$M_4(n) = M_4(n-1) + \mu \cdot (x^4(n) - M_4(n-1)), \quad \forall n \in [2; N] \quad (3)$$

where the initial moment is set as $M_4(1) = x^4(1)$. This detector may be seen as a complementary tool to the online energy detector: the periods where the energy is constant may be associated to high values of M_4 indicating nonGaussian periods, *i.e.* the presence of transients. This third detector is then a combination of a butterworth high-pass filter at frequency 500 Hz followed by the online fourth-order detector, the step being fixed to $\mu = 0.1$.

4.4. Fourth-order cumulant with prior filtering

Considering a zero-mean random variable X describing the process, its fourth-order cumulant is expressed as:

$$C_4 = \mathcal{E}\{X^4\} - 3\mathcal{E}\{X^2\}^2 \quad (4)$$

The online estimation of the C_4 basically requires the estimation of the fourth-order moment as well as the second-order moment (energy). So, estimation errors are not only due to the fourth-order moment estimator but also to the second-order moment estimator. To get a direct online estimation of the fourth-order cumulant and to make the estimation robust with respect to the second-order moment estimation, the adaptive version of this estimator described in [AMB95] is processed:

$$\begin{cases} E(n) = E(n-1) + \mu \cdot (x^2(n) - E(n-1)) \\ C_4(n) = C_4(n-1) + \gamma \cdot (x^4(n) - 3x^2(n)E(n-1) - C_4(n-1)) \end{cases} \quad (5)$$

In the below presented experiments, the steps are fixed to $\mu = 0.05$ and $\gamma = 0.01$.

For this fourth detector, the 500 Hz high-pass filter is also applied prior to the calculation of the fourth-order cumulant.

4.5. Wavelet transform and kurtosis

In the frequency domain, transients produce local high coefficients because of their oscillatory components. The non-Gaussian property of the transients is therefore enhanced in the transformed domain whereas the noise which is Gaussian remains Gaussian. This property is used to get an adaptive segmentation of the data in the time domain using Malvar wavelet decomposition. This segmentation acts like a pre-detection of transient signals. Indeed, the idea is to get large temporal segments for stationary periods corresponding to the noise only condition (with Gaussian coefficients) whereas short temporal segments are obtained when nonstationary periods appear due to the presence of any transient (with non-Gaussian coefficients). The segmentation is a data driven procedure that is achieved according to the Gaussianity nature of wavelet coefficients, using the split and merge algorithm [WIC94]. The total record duration must have a number of samples that is a power of two in order to consider a dyadic partition of the sequence. At the beginning, the finest equal size temporal segmentation is considered and wavelet coefficients are computed. At the next level, wavelet coefficients are computed for twice longer segments until reaching the total sequence duration. To get a non redundant time frequency representation, a selection of wavelet coefficients (i.e. nodes in the tree structure) is achieved. The algorithm is the following: at a given level, if the wavelet coefficients of two consecutive segments are Gaussian, then merge them. Otherwise let them dissociated. In this procedure, the fourth-order cumulant is measured to zero for making the Gaussian / non-Gaussian decision. Practically, the comparison to zero is achieved using the Byenaymé-Tchebychev inequality, considering the number of coefficients at the current level and a confidence percentage value in the decision making (90% taken in the simulations). The same procedure continues with the following two by two segments, at the considered level. When splitting, the highest cumulant node value is marked (except at the leaf level where the two nodes are marked) and replaces the father node value. This is for keeping a local high non-Gaussianity trace. This procedure is repeated from the leafs (32 samples segments) to the root (1 segment with all the samples) of the tree structure. The marked nodes permit to select the best adapted wavelet decomposition basis. Then the kurtosis values of the retained coefficients are computed to form the detection curve [Rav98].

4.6. Wavelet packet decomposition

According to [RAV01], the wavelet packet decomposition acts like a filtering that is adapted to the statistical data content. The algorithm steps are described as follows. First, a denoising procedure based on wavelet packet decomposition is achieved. This procedure only keeps frequency bands that are non-Gaussian, which allows dealing with the important low frequency components due to the pink noise. A denoised version of the data is computed by inverse transforming selected coefficients of the wavelet packet decomposition. Both wavelet packet decomposition and coefficient selection are based on a kurtosis computation criterion. Secondly, adaptive energy values are evaluated along the time on the denoised signal yielding a temporal detection curve. The Daubechies wavelet (order 16), a decomposition depth of 8 and a confidence percentage of 99% have been fixed for the simulations.

4.7. Test method

The performance of the proposed detectors is evaluated with the Receiver Operating Characteristic (ROC) curves, through a Monte Carlo set of experiments. The ROC curve is the representation of the detection rate Pd as a function of the false alarm rate Pfa . Any detection threshold applied at the output of the receiver is associated to a value of the couple (Pfa, Pd) . The ROC curve is the location of the (Pfa, Pd) points obtained when changing the detection threshold [WHA71]. The experiments are carried out for all types of transients presented in section 3.2. For the experiments, each type of transient is defined as a unique pattern $x_f(n)$ which is a “clean” transient extracted from the vibrations of a damaged module.

In order to estimate the Pd and Pfa probabilities, the noise only condition and the transient plus noise condition have to be created. The detector under test is then applied to a set of 250 synthetic observations $y(n) = n(t)$ or $y(n) = x_f(n) + n(t)$ with a desired signal-to-noise ratio (SNR). For each observation, the noise

sequence $n(t)$ is a temporal slice extracted from the vibrations of undamaged modules. A detection is decided when the receiver output is greater than a given threshold. Counting the number of detections gives an estimation of the Pfa and Pd values under the noise only condition and the transient plus noise condition respectively.

A typical detector under test is characterized by a ROC curve which is located between the blue curve (ideal detector) and the red curve (poorest detector which is a chance line) as illustrated in Figure 10. A global efficiency measure of the detector can be evaluated as the area located between the curve of the detector under test and the poorest detector, divided by the area of the upper triangle of the graph. For an ideal detector, this parameter would be equal to one, whereas for the worst possible detector it would be zero. This parameter allows an easy comparison between different detectors and will be denoted by “mean performance” of the detector.

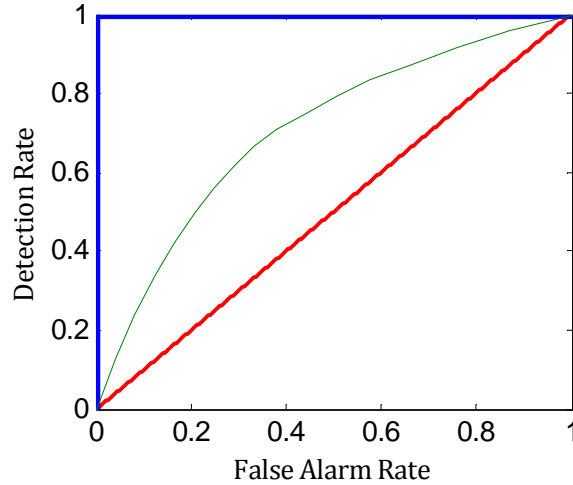


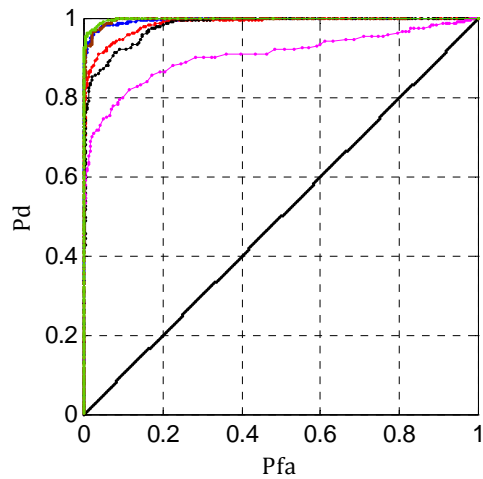
Figure 10: Example of a typical ROC curve (green line). This curve is located between the ideal curve (blue line) and the poorest one (red line). This latter is denoted chance line in the text.

4.8. Experimental results

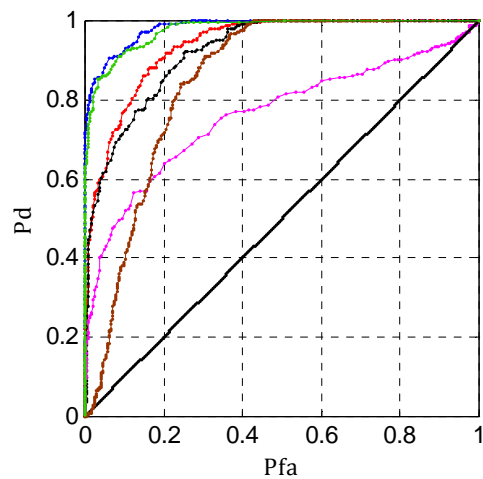
The ROC curves of all the proposed detectors are presented on Figure 11 for SNR=0 dB. The mean performance of the detectors are given on Figure 12. Without any surprise, rather poor results are obtained with the energy detector which uses few of the available information about transient features. It can be noted from these figures that high-pass filtering the data efficiently improves the results obtained by this very simple method. After filtering, the basic use of fourth-order moment does not improve the detection performance with respect to the use of second-order moment. Taking into account both statistics in the robust fourth-order cumulant estimation greatly helps improving the detection performance, especially for A and B transient types. For all the transient types except to the type E, the Malvar wavelet decomposition permits a better detection than the temporal detectors. This can be explained by the fact that the type E transient is more widely spread in the time-frequency plane than the others preventing a correct adapted wavelet decomposition. Note also that none of the methods really makes better than of the high-pass filtering and energy computation method. Due to a difficult time-frequency signature, the other proposed methods have no positive effect on type E transient detection. The results concerning the wavelet packet are disappointing (except for the type A transient). Indeed, the method sometimes suppresses frequency bands that correspond to transient content and is also not able to systematically suppress the low energy frequency bands.

All these results are summed up on Figure 12. The wavelet packet results and have not been reported on this figure. The best method among those that have been tested remains the Malvar wavelet transform detector, whose detection rate is above 96% in all cases and reaches 99% for the type A transient. The fourth-order cumulant is also very interesting since the results look very similar. This method has the advantage to be computationally low-cost but suffers from the parameters adjustment. For example, the type B "slup" transient and the E "tap-tap" transient show comparable results, *i.e.* 96% and 95% respectively. With the parameters choice $\mu = 0.01$ and $\gamma = 0.005$ (instead of $\mu = 0.05$ and $\gamma = 0.01$ previously), the results are very different, *i.e.* 89% and 98% respectively (not shown here).

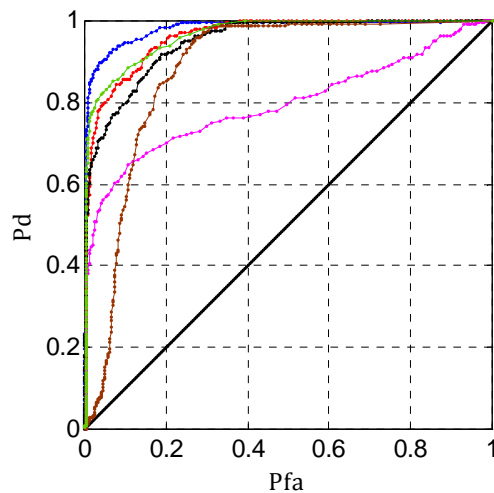
Note that the 0dB SNR simulates very poor operating conditions, since the real SNR is most of the time far above that value.



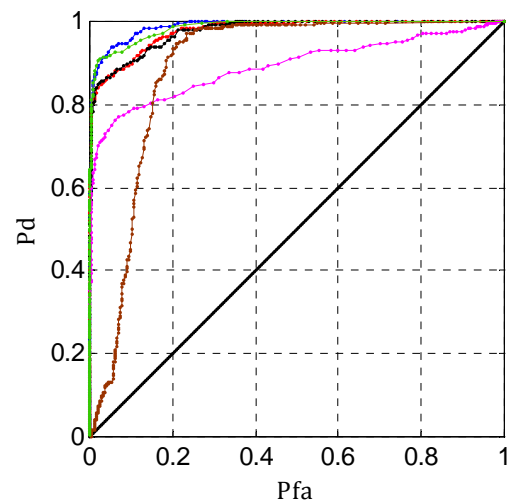
11-A Type A transient "glou-glou"



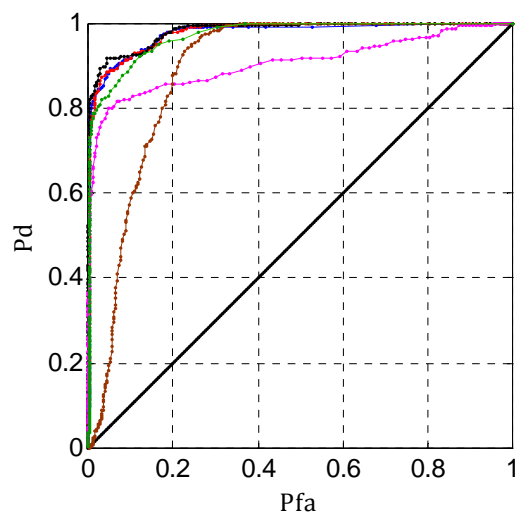
11-B Type B transient "slup"



11-C Type C transient "tic-tic"



11-D Type D transient "tac-tac"



11-E Type E transient "tap-tap"

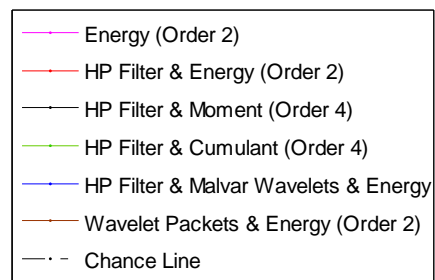


Figure 11: ROC curves of the proposed detectors for the five types of transients, SNR = 0 dB.

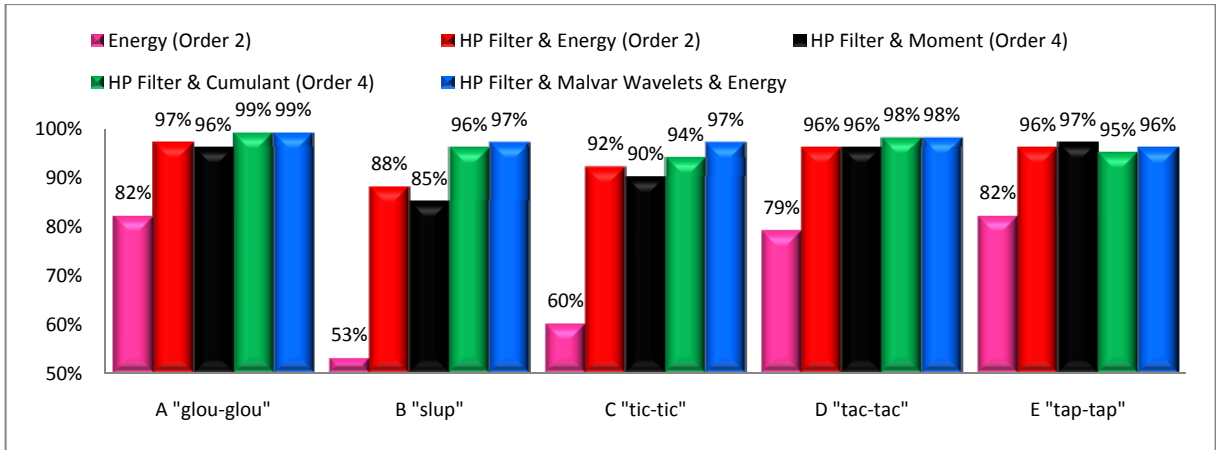


Figure 12: Mean performance of the tested detectors for each type of transient, SNR=0dB.

Three detectors have been applied on a real data sequence. On the example shown on Figure 13, the Malvar wavelet decomposition method clearly shows the presence of weak transients in comparison with the simple energy detector, even after band-pass filtering in the 200-2000 Hz frequency band. The presence of transients is accredited by human expertise and corroborated by time-frequency representations.

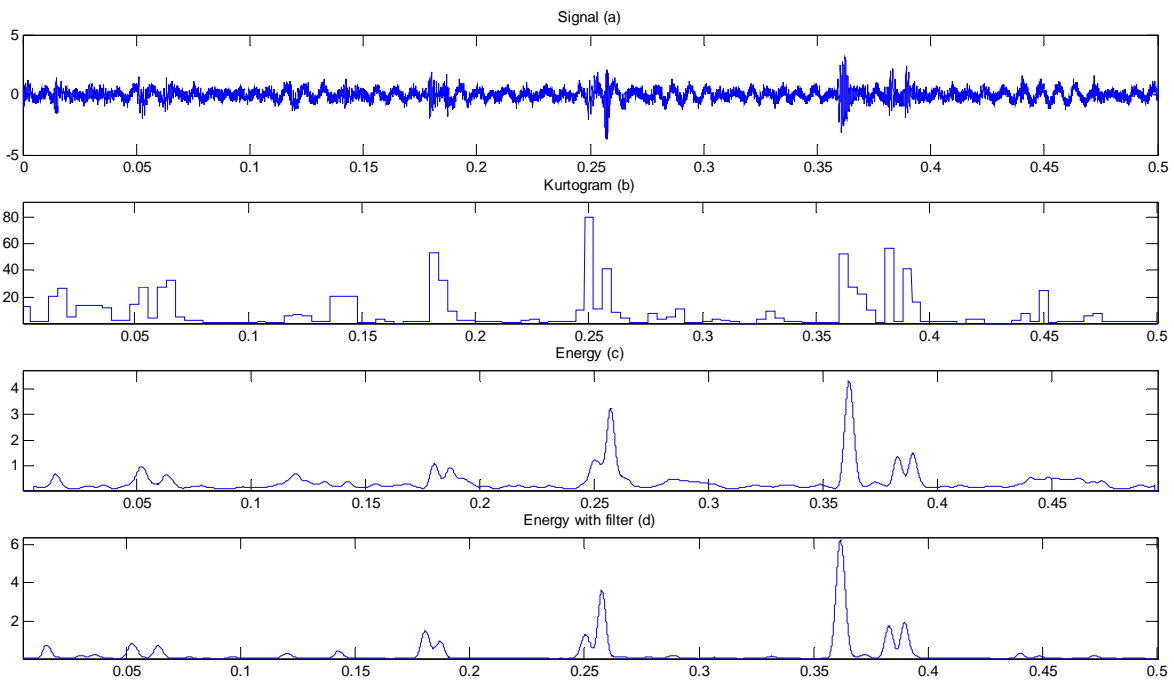


Figure 13: (a) Time representation of a damaged module (b) Energy of the Malvar wavelet decomposition basis coefficients (c) Energy of the time representation (d) Energy of the time representation after 200-2000 Hz band-pass filtering.

5. Conclusion

In this paper, we presented a feasibility study concerning the development of an automated diagnosis device for water ultrafiltration modules. Several detectors have been proposed for the detection of transient signals that are distinctive of damaged filtration fibers. Some Monte Carlo simulations have been performed over simulated signals constructed from real life recordings. These simulations showed that one of the detectors based on Malvar wavelet decomposition gives better results than any other for most of the transients to be detected. Providing the parameters are properly tuned, the fourth-order cumulant based detector also allows detection of

very weak transients in ambient noise. However, this kind of test is not sufficient and needs testing the algorithms on long time continuous real data sequences. This approach needs the creation of annotated database which is not an easy task because of uncertainties in human diagnosis. The work is under progress. Moreover, at the time being, the tested method cannot identify the class of the detected transients. Other methods are under investigation for this classification problem.

The presented results are preliminary since occurrence behaviors of the transients have not been taken into account for a precise diagnosis of the modules. The occurrence of transients may be continuous along the time with a specific mean delay between two occurrences. On the contrary, when a bubble appears, a volley of transients may be sporadically detected. Lastly, other indicators like the air pressure decrease velocity during the integrity test procedure, can be merged to the transients detection procedure in order to improve the decision making.

References

- [AMB95] Amblard P.-O., Brossier J.-M., Adaptive estimation of the fourth-order cumulant of a white stochastic process, *Signal Processing* 42 (1995) 37-43.
- [GUO10] Guo H., Wyart Y., Perot J., Nauleau F., Moulin P., Low-pressure membrane integrity tests for drinking water treatment: A review, *Water Research* 44 (2010) 41-57.
- [NIK93] Nikias C., Petropulu A., Higher-Order spectra analysis, Prentice Hall Signal Processing Series, 1993.
- [RAV98] Ravier P., Amblard P.-O., Combining an adapted wavelet analysis with fourth-order statistics for transient detection, *Signal Processing* 70 (1998) 115-128.
- [RAV01] Ravier P., Amblard P.-O., Wavelet packets and de-noising based on higher-order-statistics for transient detection, *Signal Processing* 81 (2001) 1909-1926.
- [WHA71] Whalen A. D., Detection of signals in noise, Electrical Science Series, Academic Press, 1971.
- [WIC94] Wickerhauser M. V., Adapted wavelet analysis from theory to software, A. K. Peters Wellesley, Massachussetts, 1994.